Integrating Multi-Redox Centers into one Framework for High Performance Organic Li-Ion Battery Cathode

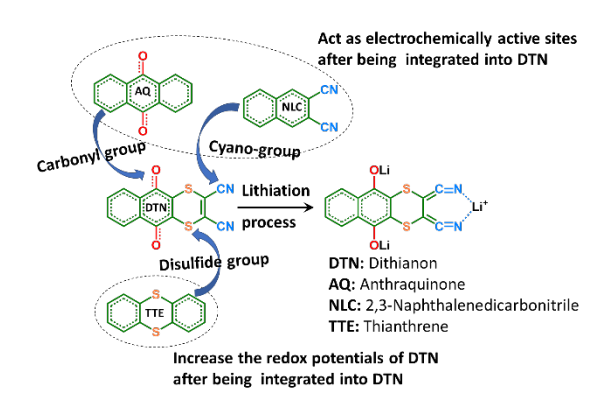
Chunyu Cui, Xiao Ji, Peng-Fei Wang, Gui-Liang Xu, Long Chen, Ji Chen, Hacksung Kim, Yang Ren, Fu Chen, Chongyin Yang, Xiulin Fan, Chao Luo, Khalil Amine, and Chunsheng Wang*

- ^a Department of Chemical and Bimolecular Engineering, University of Maryland, College Park, MD 20742, United States.
- ^b Chemical Sciences and Engineering Division, Argonne National Laboratory, 9700 South Cass Avenue, Lemont, IL 60439, United States.
- ^c Center for Catalysis and Surface Science, Northwestern University, Evanston, Illinois 60208, United States.
- ^d X-ray Science Division, Advanced Photon Source, Argonne National Laboratory, 9700 South Cass Avenue, Lemont, IL 60439, United States.
- Department of Chemistry and Biochemistry, University of Maryland, College Park, MD 20742, United States.
- Department of Chemistry and Biochemistry, George Mason University, VA 22030, United States.

⁸ Materials Science and Engineering, Stanford University, Stanford, CA 94305, United States.

ABSTRACT

Organic cathode materials are promising for developing high-energy and high-power Li-ion batteries (LIBs) due to high sustainability, low cost and heavy metal-free features. However, the energy storage of most organic cathodes relies on the electron transfer of a single type of functional group, leading to either a low redox potential or a low capacity. Here we propose a new strategy for the structure design and performance optimization of organic materials. A new organic cathode, dithianon (DTN), containing three functional groups (-S-, C=O, C N) in one framework, is reported. The -S- group increases the redox potential to 3.0 V, while C=O and C N groups enable three Li-ions involved redox reaction. As a cathode, DTN delivers 270.2 mAh g¹ at 0.5C for 300 cycles. Even at 5C, it still retains 161.5 mAh g¹ after 1000 cycles. The high-capacity, high-power and stable DTN cathode offers great promise for high performance and sustainable LIBs.



Li ion batteries (LIBs) have become dominant energy-storage devices for portable electronics since its first commercialization in 1990s,¹² and now are penetrating to electric vehicles and smart grids. The energy density and power density of state-of-the-art LIBs are limited by the low energy density of intercalation-type cathodes. Considerable research efforts have been devoted to increasing the energy density and power density of intercalation-type transition-metal oxide cathodes (e.g., LiCoO₂, LiFePO₄, LiNi_{0.8}Mn_{0.1}Co_{0.1}O₂ and Li-rich cathodes),^{3.8} and the capacities of intercalation-type transition-metal oxide cathodes are approaching to their capacity limit of ~200 mA h g⁴.

As alternatives to the inorganic counterparts, organic cathode materials are promising candidates for high energy and high power density LIBs due to the tunable molecular structure and high structural diversity. 9-10 The reversible redox reactions of organic materials involve the charge state change of the electrochemically active organic functional groups such as carbonyl group (C=O), imine group (C=N), organic free radicals, disulfide group (S-S), azo group (N=N), and cyano-group (C N). 11-21 Up to date, a number of carbonyl group-based organic materials (oxocarbon salts, 22 poly-(anthraquinonyl sulfide)23 and polyimide24) and imine group-based organic materials (triquinoxalinylene²³ and alloxazine²⁶) have been reported for LIB cathodes. Among them, the organic cathode, cyclohexanehexone, can even reach an ultrahigh capacity up to 902 mA h g⁺, ²⁷ which is over four times higher than most of intercalation-type transition-metal oxide cathodes. Zhiqiang Luo et al. reported a two-dimensional microporous covalent organic framework, poly(imide-benzoquinone), polymerized with graphene as a high rate organic cathode for LIBs.28 Nevertheless, the poor long-term cycling stability, sluggish reaction kinetics and low redox potential limit the large-scale application of organic cathode materials. Therefore, it is still challenging to develop high energy and high cyclic stability organic cathodes for sustainable LIBs.

In this work, we reported exceptional electrochemical performance of a dithianon (DTN) cathode material, consisting of two carbonyl groups, two cyano-groups and two sulfur atoms

(Figure 1a). The carbonyl group and cyano-group in DTN serve to enhance the capacity, while the heteroatom (S) in DTN is to increase the redox potentials. To confirm the electrochemical activity of each functional group, the electrochemical behaviors of organic materials with only one type of each functional group such as anthraquinone (AQ, Figure 1b), thianthrene (TTE, Figure 1c) and 2, 3-naphthalenedicarbonitrile (NLC, Figure 1d) were studied as controls. In DTN, both the carbonyl group and cyano-group act as electrochemically active sites to react with Li¹. As proposed in Figure 1e, DTN can reversibly react with three lithium ions step by step to deliver a theoretical capacity of 271.2 mA h g⁴. More importantly, the doping of heteroatoms into the organic material lowers the energy levels of the lowest unoccupied molecular orbital (LUMO), resulting in an increased redox potential.²⁰¹¹ As a cathode, the DTN retains a high reversible capacity of 270.2 mA h g⁴ after 300 cycles at 0.5C with a pair of redox plateaus centered at 3.0 V, and 161.5 mA h g⁴ after 1000 cycles at 5C. Hence, DTN with two sulfur atoms and two types of electroactive groups, is a promising organic cathode material for high performance and sustainable LIBs.

The structure and morphology of these four organic materials were characterized using scanning electron microscopy (SEM), solid state NMR, X-ray diffraction (XRD), Raman spectroscopy and Fourier-transform infrared (FTIR) spectroscopy, and thermogravimetric analysis (TGA). The SEM images in **Figure S1** demonstrate that NLC, TTE, AQ and DTN samples consist of irregular shape particles with a size in the range from 1 μm, and the sharp XRD peaks in **Figure 1**f and **S2** reveal that they display well-defined crystalline structure. The solid state ¹⁰C magic-angle spinning (MAS) NMR spectra are provided in **Figure S3**, and the different ¹⁰C resonances clearly demonstrate the typical chemical environments of C in DTN, AQ, TTE and NLC. Furthermore, the Raman spectrum of DTN in **Figure 1**g confirms the existence of -S- stretching vibration at ~ 492 cm¹⁰, ²⁰ C=O stretching vibration at ~1665 cm¹⁰, ³⁰ and the symmetric/asymmetric stretching vibrations of C N at 2215 cm³⁰ and 2230 cm³⁰, ^{304,35} Similar C=O stretching at ~1665 cm³⁰ was also observed for carbonyl groups in AQ (**Figure S4**), while the

strong fluorescence of TTE and NLC leads to the increased baseline intensity in the Raman spectra, which overlaps with their characteristic Raman peaks. The FTIR results in **Figure 1**h and **S5** provide a more explicit evidence without fluorescence disturbance, and the typical IR peaks of DTN are consistent with that in the Raman spectra. The thermostability of DTN, AQ, TTE and NLC were investigated by TGA, as shown in **Figure 1**i and **S6**, all these organic materials are stable up to ~ 200 °C.

Quantum chemistry calculations were conducted to evaluate the redox properties of the four organic materials from an atomic scale.³⁶ The highest occupied molecular orbital (HOMO) and LUMO distributions of the four organic molecules are shown in **Figure 2**, and their energies were residing on the LUMO and HOMO. The deeper LUMO level is, the better electron affinity it would exhibit. As revealed, DTN delivers much lower LUMO energy level of -5.68 eV than AQ (-1.15 eV), TTE (-3.17 eV) and NLC (-2.67 eV), suggesting DTN owns greater electron affinities, so it should exhibit a higher reduction potential than AQ, TTE and NLC. The LUMO is mainly located on the C=C double bond and the top of S atoms, suggesting their electron acceptor roles during the reduction. In addition, DTN has a much lower gap (0.14 eV) between its HOMO and LUMO levels than AQ (4.22 eV), TTE (4.19 eV) and NLC (4.49 eV), indicating DTN has the highest intrinsic electronic among these four samples.

The role of each function group in DTN was investigated by comparing the charge-discharge curves of AQ, TTE, NLC and DTN that acquired in coin-type half cells with Li metal as a counter electrode, within the voltage range of 1.0-3.5V. As shown in **Figure 3a**, AQ exhibits two pairs of redox plateaus at 2.1 V and 2.3 V, with a discharge capacity of 145.5 mAh g⁻¹, corresponding to the reversible reaction between two carbonyl groups in AQ and two Li-ions. NLC (**Figure 3b**) shows a pair of redox plateaus centered at 1.4 V, with a discharge capacity of 138.8 mAh g⁻¹, corresponding to the reversible reaction between cyano-groups in NLC and Li-ions. As for the TTE electrode in **Figure 3c**, it exhibits a long sloping discharge curve below 1.3 V, with a discharge capacity of only 8.1 mAh g⁻¹, and the charge-discharge curves of

conductive carbon black in Figure S7 reveal the capacity of TTE is totally contributed by the conductive carbon black, demonstrating TTE is electrochemically inactive at the voltage range from 1.0 to 3.5V. The CV results of AQ, TTE and NLC (Figure S8) are consistent with their charge-discharge curves. In comparison, the DTN (Figure 3d) displays a higher average discharge voltage than AQ, NLC, and TTE, with a high discharge capacity of 243.9 mAh g¹, of which a long discharge plateau at ~ 2.9 V contributes a capacity of ~90 mAh g⁻¹, and a sloping discharge curve from 2.9 V to 1.0 V contributes a capacity of ~154 mAh g⁻¹. Therefore, the electrochemical behaviors of these four organic materials demonstrate that carbonyl groups and cyano-groups are electrochemically active sites in DTN, and the redox plateaus of carbonyl groups in AQ and cyano-groups in TTE are lower than that in DTN, confirming that the doping of heteroatoms into the organic material serves to increase the redox potential. The electrochemical behaviors of DTN are consistent with the DFT results. To understand the multistep lithiation process of DTN, the structure simulation of DTN at different lithiation stages was conducted, and the optimized energy favorable structures of DTN-xLi (x = 1, 2, and 3) were attached to the discharge curve of DTN in the cutoff window from 1 3.5 V. As shown in Figure 3d, the DFT results reveal that three Li ions can be inserted into the DTN in the cutoff window from 1 to 3.5 V, referring to a theoretical capacity of 271.2 mA h g¹. Specifically, two sites of O atoms in DTN are the most energy favorable for Li-ion accommodation, corresponding to average reduction potentials of 2.9 V and 2.1 V (vs. Li/Li⁺), respectively. The third Li-ion tends to interact with the -CN groups in DTN, which exhibit the average reduction potentials of 1.4 V (vs. Li/Li⁻). The corresponding calculated energy levels of DTN at different lithiation stages were offered in **Figure S9**.

The lithiation/delithiation capacities and redox potentials of the DTN were evaluated and compared to the results from Quantum chemistry calculations, at a potential range of 1.0 [3.5 V in coin cells by using lithium metal as a counter electrode, in the electrolyte of 7 M Lithium bis(trifluoromethanesulfonyl)imide (LiTFSI) in 1,2-Dimethoxyethane (DME)/dioxolane (DOL)

(volume, 1:1), (denoted as 7M LiTFSI-DME/DOL). To further prevent the dissolution of DTN electrode in 7M LiTFSI-DME/DOL electrolyte during the long cycling process (Figure \$10), the atomic layer deposition (ALD) technique was used to deposit a thin layer (5 nm) of Al₂O₃ on DTN electrode to protect the organic material from dissolution. The typical charge-discharge curves of Al₂O₃ coated DTN electrode in the first, second, 5th and 100th cycles at 0.5 C are shown in Figure 4a, $(1C = 271.2 \text{ mAh } g^{-1})$. The gradually increase in Coulombic efficiency and discharge capacity from the first to 5th cycle is due to an activation process caused by the coating of the insulating Al₂O₃. After the initial activation process, Al₂O₃ coated DTN electrode displays a discharge capacity of 243.9 mAh g⁻⁻ and 246.4 mAh g⁻⁻ in the 5⁺ and 100⁺ cycle, with a long and flat plateau at ~2.9 V and a slopping plateau centered at 1.8 V, which is similar to the calculated potentials of DTN-1Li, DTN-2Li and DTN-3Li in Figure 3d. In addition, the electrochemical behavior of DTN was also studied by cyclic voltammetry (CV) at a scan rate of 0.1 mV s⁻, as shown in Figure 4b. A sharp peak at \sim 2.8 V and a broad peak at \sim 2.2 V were observed in the cathodic scan, corresponding to a sharp peak at ~3.3 V and a broad peak at ~2.8 V in the anodic scan. The CV results are consistent with the charge-discharge curves. Due to the use of highly concentrated electrolyte of 7M LiTFSI-DME/DOL, and the coating of an electronic nonconductive Al₂O₃ layer, the DTN deliver not completely reversible cathodic and anodic cyclic voltammogram, but the similar peak area for the oxidation and reduction peaks in figure 4b suggests high lithiation/de-lithiation reversibility and good cyclic stability of Al₂O₃ coated DTN in 7M LiTFSI-DME/DOL.

The excellent cycling stability of Al₂O₃ coated DTN cathode is shown in **Figure 4**c. As revealed, it delivers a first discharge capacity of 228.2 mA h g⁴ at 0.5C, then increases to 243.9 mA h g⁴ after 5 activation cycles and remains a reversible capacity of 270.2 mA h g⁴ after 300 cycles. The capacity fluctuation of the initial cycles in Figure 4e is caused by the Al₂O₃ coating layer on the DTN cathode. The Al₂O₃ coating layer is electronic nonconductive, so it reduces the

electronic conductivity of the DTN cathode, decreasing the reaction kinetics. In addition, it increases the lithium ion transfer pathway from the electrolyte to the DTN cathode, resulting in enhanced interfacial impedance between electrode and electrolyte. An initial activation process is required to promote the electron and Li-ion transfer in the DTN cathode, which is also observed in the other literature.³⁷ The capacity fluctuation in the long-term cycling is due to the environmental temperature variation during the battery test. To further confirm it, the electrochemical impedance spectroscopy (EIS) from the 1st cycle to 100st cycle was performed. As shown in Figure S11, the depressed semi-circle represents the interphase resistance, which decreases from ~180 Ohm to ~120 Ohm after 5th cycle due to the initial activation process. Then, it increases to ~170 Ohm from 5th to 20th cycle, and stabilizes at ~150 Ohm after 50th cycles, demonstrating the stable interphase layer of DTN cathode for the reversible lithiation/delithiation process. The rate capability of DTN at various current densities from 0.2C to 15C was also evaluated. As shown in **Figure 4**d, with the elevated current densities from 0.2C to 15C, DTN exhibits the average reversible capacities of 285.8, 276.4, 260.3, 239.1, 212.8, 184.4 and 153.6 mA h g⁻¹ at 0.2C, 0.5C, 1C, 2C, 5C, 10C and 15C, respectively. When the current density is reduced back to 0.2C, the capacity of DTN recovers to 281.2 mA h g₁, comparable to its initial value. Moreover, the long-term cycling performance of DTN at a high current density of 5C was evaluated and shown in Figure 4e. It delivers an initial discharge capacity of 184.3 mAh g⁻¹ and retains a reversible capacity of 161.5 mA h g1 after 1000 cyles, demonstrating a powerful robustness at the high current density. The superior electrochemical performance of DTN is not only beneficial from its structural property, but also closely related to its reaction kinetics. Thus, the CV curves at different sweep rates from 0.1 to 2.0 mV s¹¹ were conducted to analyze the reaction kinetics of the DTN cathode. As shown in Figure S12, with the increased scan rate, the anodic peak shifts to a lower value, while the cathodic peak shifts to a higher value due to the enhanced polarization. According to the equation proposed by Dunn et al,38.39 the k1 and k2 constants are 0.76 and 0.82 based on the anodic scan (Figure S13a) and cathodic scan (Figure

\$13b), suggesting that the exceptional rate capability of DTN cathode is attributed to its surface-dominated pseudocapacitance mechanism.

The structure evolution of DTN at different states of discharge and charge was investigated by the ex situ Raman spectra (Figure 5a and b). When the DTN electrode is discharged to 2.0 V, the strong peak at 1665 cm⁻¹ attributed to the C=O stretching vibration is remarkably weakened (Figure 5b), while a new peak at 521 cm⁻¹ appears (Figure 5a), corresponding to the lithiated carbonyl group and formation of Li-O bond. It is well-matched with the characteristic Raman peak for Li₂O. After fully discharge to 1.0 V, the peak for C=O stretching at 1665 cm⁻¹ is completely disappeared (Figure 5b), and the peak for Li-O bond becomes stronger. Moreover, the symmetric/asymmetric stretching vibrations of C N at 2215 cm⁻¹ and 2230 cm⁻¹ are merged into a broad peak and blue-shifted, while other new peaks at 371, 392, 682, 695, 1290, 1335, 1408, 1477, 1577, and 1598 cm⁻¹ arise, which are in general agreement with the polypyrrole's Raman peaks. 40-42 The appearance of these new peaks indicates that the C N groups transform to a polypyrrole-like structure during the discharge process. The disappearance of C=O stretching vibration, the alteration of C N stretching vibration, and the appearance of these new peaks reveal the strong chemical interaction between Li⁺ and O/N in DTN at 1.0 V. When DTN is fully charged back, most Raman peaks for DTN are recovered, revealing a good reversibility of the DTN cathode during charge and discharge. The -S- stretching vibration at ~ 492 cm¹¹ is retained during the charge-discharge process, confirming that -S- group does not participate in the redox reaction. Hence, the first and second Li-ions are accommodated by the two O atoms in the carbonyl groups, and the third Li-ion is interacted with cyano-groups to form a polypyrrole-like structure. The Raman results are consistent with the proposed reaction mechanism in Figure 1e and Figure 3d. To better demonstrate the phase evolution of DTN electrode, the in situ XRD during the first discharge process was conducted (Figure 5c and 5d), and the corresponding discharge curve is shown in the left side of Figure 5c. To avoid the activation process, DTN without Al₂O₃ coating was used for in situ XRD characterization. Based on the proposed

mechanism in Figure 1e and Figure 3d, three lithiated structures are formed within the potential range from 1.0-3.5 V, which are named DTN-1Li, DTN-2Li and DTN-3Li, respectively. During the first lithiation process corresponding to the potential plateau at ~ 2.9 V, the in situ XRD results unravel that the peak at 12.7° becomes stronger, the peaks at 25.9° and 26.3° shift to 25.1° and 25.6°, respectively, a new peak at 27.9° emerges and becomes stronger, and the peaks at 28.7° and 29.0° disappear at the end of this process, indicating the phase change from DTN to DTN-1Li. Upon further lithiation process corresponding to the sloping curve from 2.7 to 1.0 V, the in situ XRD shows continuous variation tendency of peaks, in which the new peaks at 12.0° and 24.3° emerge and become stronger, and peaks at 12.7°, 25.1°, 25.6° and 27.9° turn to be weaker. Therefore, the crystal structure of DTN-3Li is analogous to that of DTN-2Li. By combining the information from in situ XRD patterns and DFT calculations in Figure 3d, we conclude that DTN mainly delivers two parts of structural evolution during its lithiation process. The initial lithiation process experiences the phase transformation from DTN to DTN-1Li at the potential plateau of 3.0-2.7 V, and the further lithiation is accompanied with continuous phase change from DTN-1Li to DTN-3Li in a sloping potential range of 2.7-1.0 V. The in situ XRD and ex situ Raman results clearly demonstrate the structure evolution and reversible lithiation/de-lithiation mechanism of the DTN cathode.

In conclusion, DTN as a new organic cathode material was reported for sustainable and high-performance LIBs. The DFT calculations and experimental results unravel that two kinds of organic functional groups, carbonyl group and cyano group, in DTN act as electrochemically active sites to react with three Li-ions in the potential range from 1[3.5 V, and the introduction of the heteroatom (S) into the DTN enhances its redox potentials. The DTN-based cathode delivers a reversible capacity 270.2 mA h g⁺ at 0.5C after 300 cycles and retains a reversible capacity of 161.5 mA h g⁺ at 5C for 1000 cycles. The *ex situ* Raman and *in situ* XRD spectra reveal its structure and phase evolution during discharge and charge process, and confirm its exceptional structure reversibility and stability. Therefore, this work not only provides a new

promising organic cathode material (DTN), but also offers a new structure design and

performance optimization stratedgy by incorporating multi-redox centers in one framework to

enhanced the redox potential and capacity of organic electrode materials for sustainable and

high-performance LIBs.

ASSOCIATED CONTENT

Supporting Information.

Experimental details, SEM images, XRD patters, NMR spectra, Raman spectra, FTIR spectra,

TGA, charge-discharge curves, CV curves, calculated energy lever at different lithiation stages,

cyclic performance, Nyquist plots, CV curves at various sweep rates and corresponding peak

current I_p as a function of square root of scan rate $V^{1/2}$.

AUTHOR INFORMATION

Corresponding Author

* E-mail: cswang@umd.edu; cluo@gmu.edu

Notes

The authors declare no competing financial interest.

ACKNOWLEDGMENT

We acknowledge the support of the Maryland NanoCenter and its NispLab. The NispLab is

supported in part by the NSF as a MRSEC Shared Experimental Facility. We also acknowledge

the support from the Nanostructures for Electrical Energy Storage (NEES), an Energy Frontier

Research Center funded by the US Department of Energy, Office of Science, Basic Energy

Sciences, under Award number DESC0001160. G. Xu and K. Amine gratefully acknowledge

support from the U.S. Department of Energy (DOE), Office of Energy Efficiency and Renewable

Energy, Vehicle Technologies Office. This research used resources of the Advanced Photon

Source, an Office of Science User Facility operated for the U.S. Department of Energy (DOE) Office of Science by Argonne National Laboratory, and was supported by the U.S. DOE under Contract No. DE-ACO-06CH11357. H.K (Raman work) was supported by the US Department of Energy, Office of Basic Energy Sciences, through grant DE-FG02-03ER15457 to the Institute for Catalysis for Energy Processes (ICEP) at Northwestern University. C. Luo acknowledges the support from George Mason University, Award No. 183904. We thank the National Science Foundation (NSF 1726058) for for solid state NMR funding.

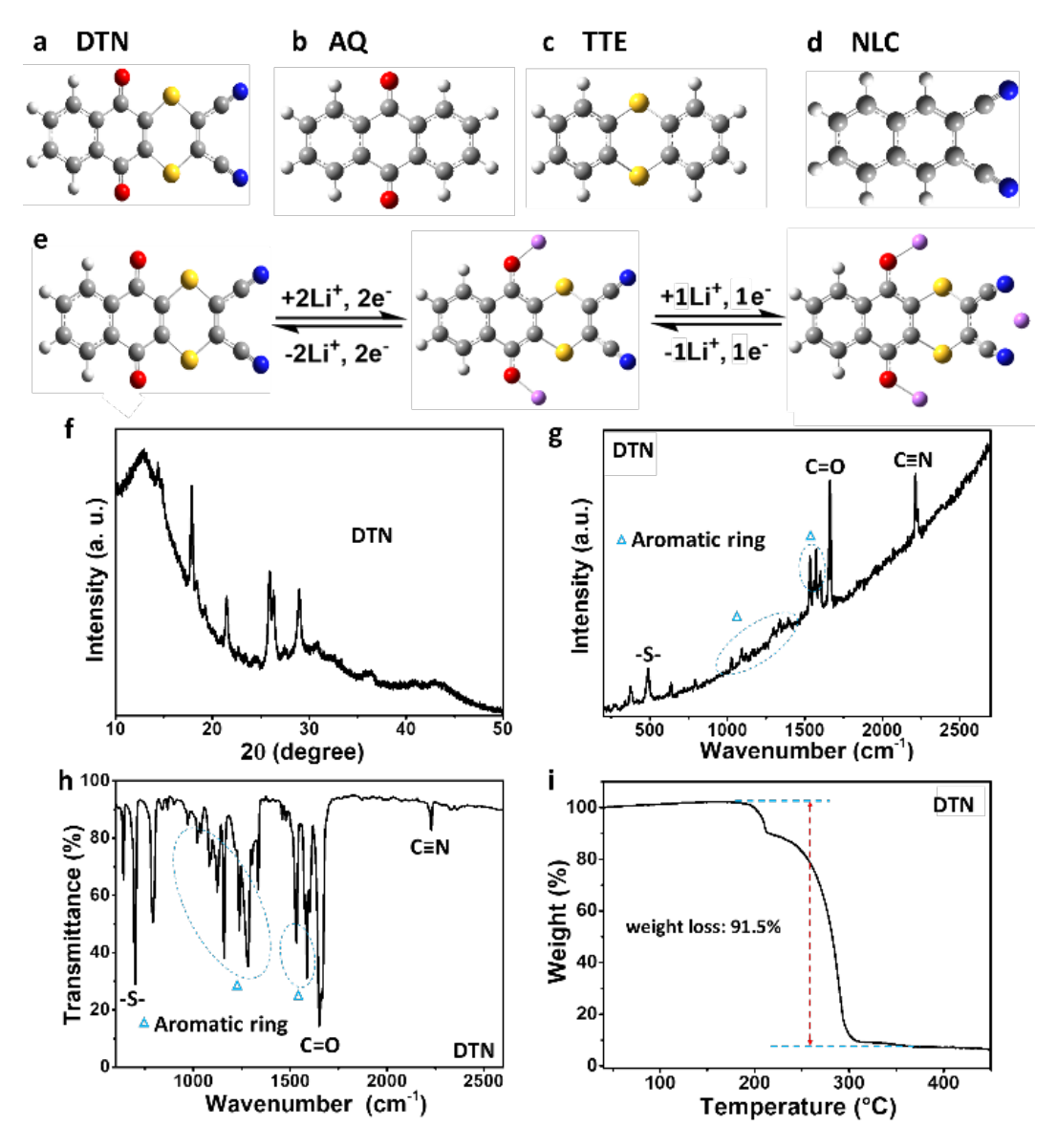


Figure 1. Structural Demonstration and Investigation. (a-d) The structure of dithianon (DTN, a), anthraquinone (AQ, b), thianthrene (TTE, c) and 2, 3-naphthalenedicarbonitrile (NLC, d). (e) The proposed reaction mechanism of DTN for LIBs with three Li ion participated in. The white, grey, red, yellow, pink and blue balls represent the H, C, O, S, Li and N atoms, respectively.(f-i) The XRD (f), Raman (g), FTIR (h), and TGA (i) results of DTN. The Raman spectra show consistent peaks with the FTIR. The TGA reveal that the weight loss of DTN proceeds in two stages.

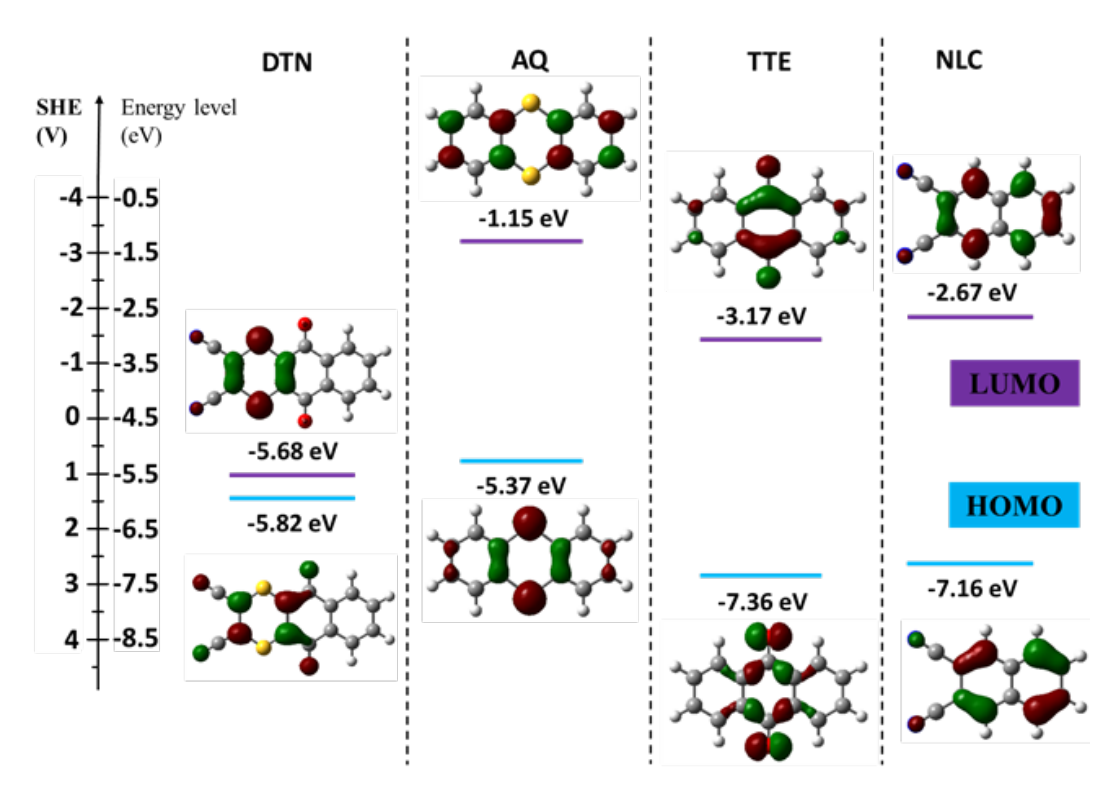


Figure 2. Quantum Chemistry Calculation. Quantum chemistry calculated electronic structures and relative energies using B3LYP/6-31+G(d, p) in acetone solvent, the left axis represents the relative voltage (versus SHE) and the right axis stands for the relative energy level in vacuum. The dark red and dark green regions represent the deletion and accumulation of electrons, respectively.

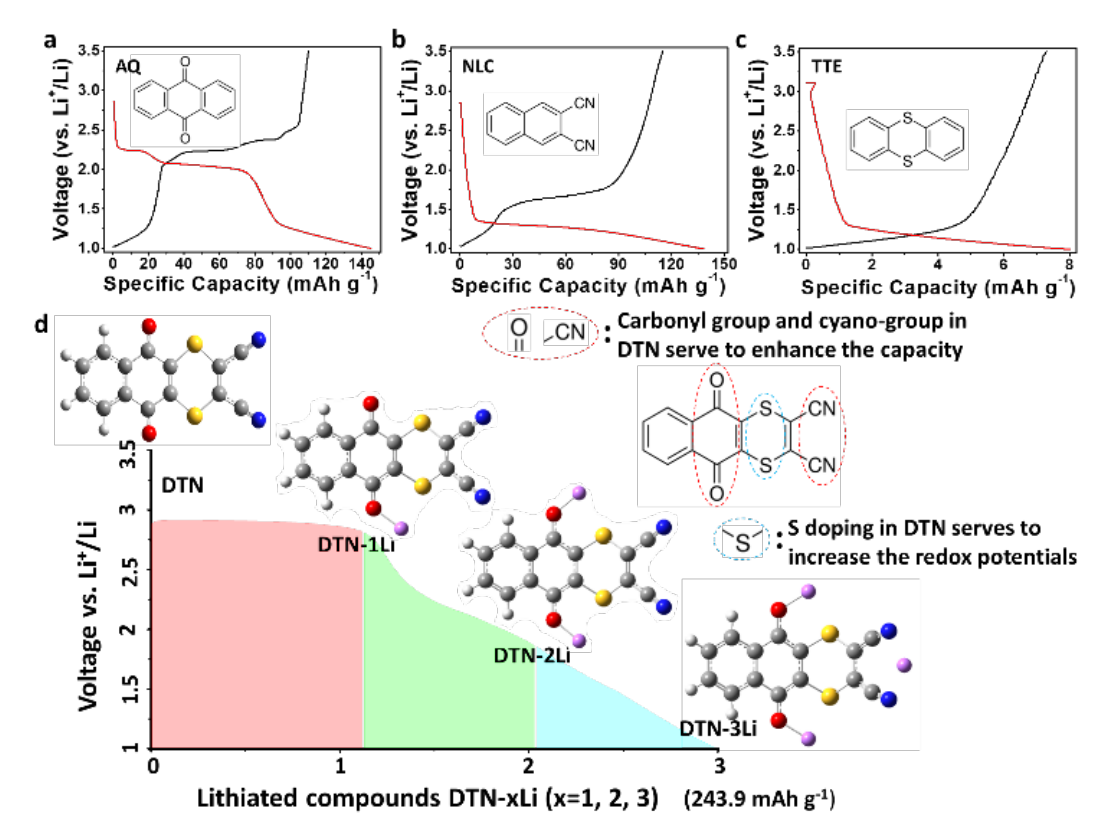


Figure 3. Electrochemical Comparison and Predicted Structural Evolution during Lithiation Process. (a-c) The charge-discharge curves of AQ (a), NLC (b) and TTE (c) in the cutoff window from 1.0 V to 3.5 V, at 0.2C.(d) The discharge curve of DTN in the cutoff window from 1.0 V to 3.5 V, and the predicted lithiated structures during the discharge process.

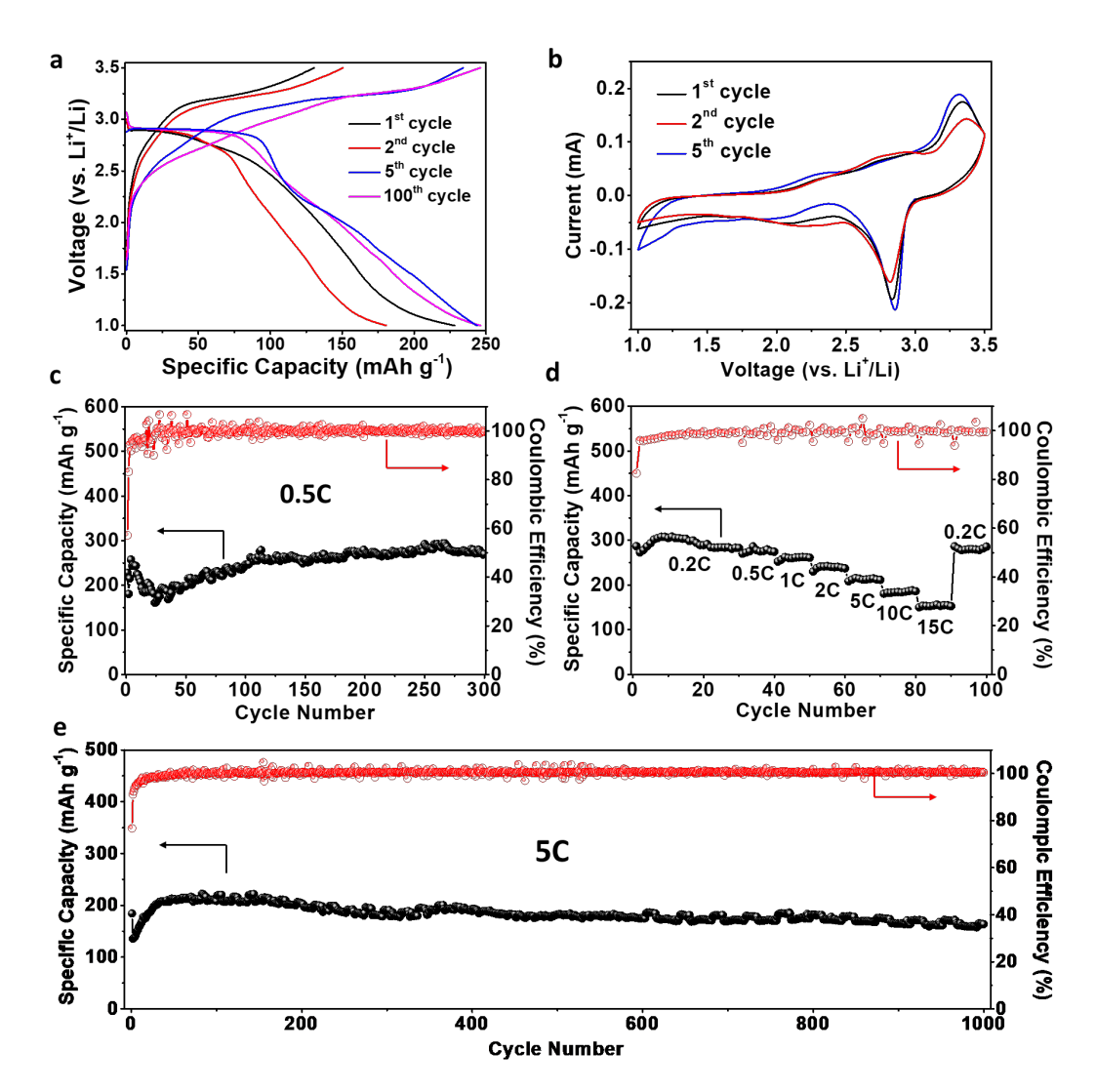


Figure 4. Electrochemical Properties of DTN. (a) The charge-discharge curves of DTN in the cutoff window from 1.0 V to 3.5 V. (b) The cyclic voltammetry of DTN with the scan rate of 0.1 mV s-1. (c) The cycling performance of DTN cathode at 0.5C. (d) The rate capability of DTN cathode at various current densities from 0.2C to 15C. (e) The cycle performance of DTN cathode at 5C.

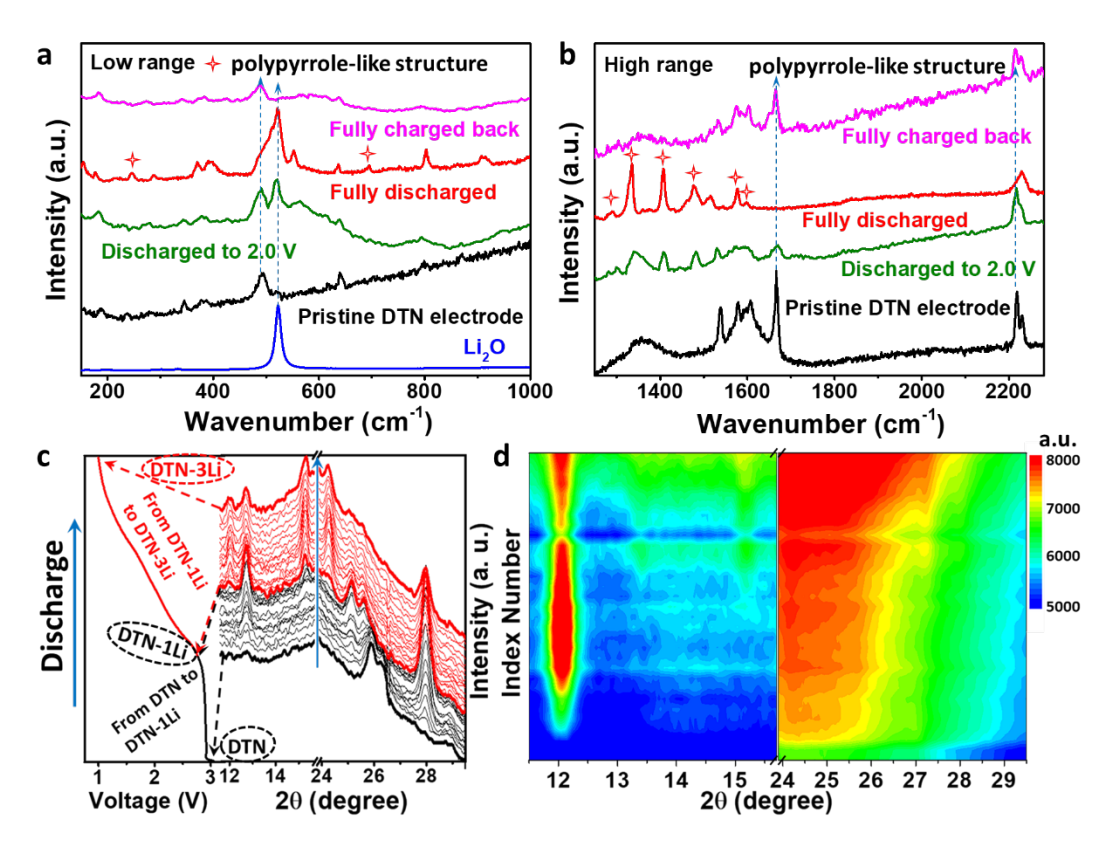


Figure 5. Structure evolution of DTN. (a-b) The (a) low range and (b) high range ex-situ Raman spectra of DTN cathode at different stages of the pristine DTN electrode before cycling, fully-discharged, discharged to the voltage of 2.0 V, and fully-charged back stage. (c-d) The in-situ XRD pattern (c) with the discharge curve, and the corresponding contour maps (d) related to the evolution of the main characteristic diffraction peaks of DTN cathode during the first discharge process. ($\lambda = 1.5416 \text{ Å}$).

REFERENCES

- 1. Armand, M.; Tarascon, J. M. Building Better Batteries. *Nature* **2008**, *451*, 652.
- 2. Nitta, N.; Wu, F.; Lee, J. T.; Yushin, G. Li-Ion Battery Aterials: Present and Future. *Mater. Today* **2015**, *18*, 252-264.
- 3. Yamada, A.; Chung, S.-C.; Hinokuma, K. Optimized LiFePO₄ for Lithium Battery Cathodes. *J. Electrochem. Soc.* **2001**, *148*, A224-A229.
- 4. Ohzuku, T.; Makimura, Y. Layered Lithium Insertion Material of LiNi_{1/2}Mn_{1/2}O₂: A Possible Alternative to LiCoO₂ for Advanced Lithium-ion Batteries. *Chem. Lett.* **2001**, *30*, 744-745.
- 5. Cabana, J.; Monconduit, L.; Larcher, D.; Palacin, M. R. Beyond Intercalation-Based Li-Ion Batteries: the State of the Art and Challenges of Electrode Materials Reacting Through Conversion Reactions. *Adv. Mater.* **2010**, *22*, E170-E192.
- 6. Luo, K.; Roberts, M. R.; Guerrini, N.; Tapia-Ruiz, N.; Hao, R.; Massel, F.; Pickup, D. M.; Ramos, S.; Liu, Y.-S.; Guo, J. Anion Redox Chemistry in the Cobalt Free 3d Transition Metal Oxide Intercalation Electrode Li[Li_{0.2}Ni_{0.2}Mn_{0.6}]O₂. *J. Am. Chem. Soc.* **2016**, *138*, 11211-11218.
- 7. Li, J.; Downie, L. E.; Ma, L.; Qiu, W.; Dahn, J. Study of the Failure Mechanisms of LiNi_{0.8}Mn_{0.1}Co_{0.1}O₂ Cathode Material for Lithium Ion Batteries. *J. Electrochem. Soc.* **2015**, *162*, A1401-A1408.
- 8. Zuo, Y.; Li, B.; Jiang, N.; Chu, W.; Zhang, H.; Zou, R.; Xia, D. A High-Capacity O₂-Type Li-Rich Cathode Material with a Single-Layer Li₂MnO₃ Superstructure. *Adv. Mater.* **2018**, *30* (16), 1707255.
- 9. Lee, S.; Kwon, G.; Ku, K.; Yoon, K.; Jung, S. K.; Lim, H. D.; Kang, K. Recent Progress in Organic Electrodes for Li and Na Rechargeable Batteries. *Adv. Mater.* **2018**, 1704682.
- 10. Schon, T. B.; McAllister, B. T.; Li, P.-F.; Seferos, D. S. The Rise of Organic Electrode Materials for Energy Storage. *Chem. Soc. Rev.* **2016**, *45*, 6345-6404.
- 11. Liang, Y.; Tao, Z.; Chen, J. Organic Electrode Materials for Rechargeable Lithium Batteries. *Adv. Energy Mater.* **2012**, *2*, 742-769.
- 12. Deng, Q.; He, S.-J.; Pei, J.; Fan, C.; Li, C.; Cao, B.; Lu, Z.-H.; Li, J. Exploitation of Redox-Active 1, 4-Dicyanobenzene and 9, 10-Dicyanoanthracene as the Organic Electrode Materials in Rechargeable Lithium Battery. *Electrochem. Commun.* **2017**, *75*, 29-32.
- 13. Lu, Y.; Zhang, Q.; Li, L.; Niu, Z.; Chen, J. Design Strategies toward Enhancing the Performance of Organic Electrode Materials in Metal-Ion Batteries. *Chem* **2018**, *4*, 2786-2813.
- 14. Song, Z.; Zhou, H. Towards Sustainable and Versatile Energy Storage Devices: an Overview of Organic Electrode Materials. *Energ. Environ. Sci.* **2013**, *6*, 2280-2301.
- 15. Häupler, B.; Wild, A.; Schubert, U. S. Carbonyls: Powerful Organic Materials for Secondary Batteries. *Adv. Energy Mater.* **2015**, *5*, 1402034.
- 16. Armand, M.; Grugeon, S.; Vezin, H.; Laruelle, S.; Ribière, P.; Poizot, P.; Tarascon, J.-M. Conjugated Dicarboxylate Anodes for Li-ion Batteries. *Nat. Mater.* **2009**, *8*, 120.
- 17. Liang, Y.; Jing, Y.; Gheytani, S.; Lee, K.-Y.; Liu, P.; Facchetti, A.; Yao, Y. Universal Quinone Electrodes for Long Cycle Life Aqueous Rechargeable Batteries. *Nat. Mater.* **2017**, *16*, 841.
- 18. Wu, Y.-L.; Horwitz, N. E.; Chen, K.-S.; Gomez-Gualdron, D. A.; Luu, N. S.; Ma, L.; Wang, T. C.; Hersam, M. C.; Hupp, J. T.; Farha, O. K. G-Quadruplex Organic Frameworks. *Nat. Chem.* **2017**, *9*, 466.

- 19. Song, Z.; Qian, Y.; Gordin, M. L.; Tang, D.; Xu, T.; Otani, M.; Zhan, H.; Zhou, H.; Wang, D. Polyanthraquinone as a Reliable Organic Electrode for Stable and Fast Lithium Storage. *Angew. Chem. Int. Eit.* **2015**, *127*, 14153-14157.
- 20. Nokami, T.; Matsuo, T.; Inatomi, Y.; Hojo, N.; Tsukagoshi, T.; Yoshizawa, H.; Shimizu, A.; Kuramoto, H.; Komae, K.; Tsuyama, H. Polymer-Bound Pyrene-4, 5, 9, 10-Tetraone for Fast-Charge and-Discharge Lithium-Ion Batteries with High Capacity. *J. Am. Chem. Soc.* **2012**, *134*, 19694-19700.
- 21. Park, M.; Shin, D. S.; Ryu, J.; Choi, M.; Park, N.; Hong, S. Y.; Cho, J. Organic Catholyte Containing Flexible Rechargeable Lithium Batteries. *Adv. Mater.* **2015**, *27*, 5141-5146.
- 22. Chen, H.; Armand, M.; Demailly, G.; Dolhem, F.; Poizot, P.; Tarascon, J.-M. From Biomass to a Renewable LiXC₆O₆ Organic Electrode for Sustainable Li-Ion Batteries. *ChemSusChem* **2008**, *1*, 348-355.
- 23. Song, Z.; Zhan, H.; Zhou, Y. Anthraquinone Based Polymer as High Performance Cathode Material for Rechargeable Lithium Batteries. *Chem. Commun.* **2009**, *4*, 448-450.
- 24. Song, Z.; Xu, T.; Gordin, M. L.; Jiang, Y.-B.; Bae, I.-T.; Xiao, Q.; Zhan, H.; Liu, J.; Wang, D. Polymer–Graphene Nanocomposites as Ultrafast-Charge and-Discharge Cathodes for Rechargeable Lithium Batteries. *Nano Lett.* **2012**, *12*, 2205-2211.
- 25. Peng, C.; Ning, G.-H.; Su, J.; Zhong, G.; Tang, W.; Tian, B.; Su, C.; Yu, D.; Zu, L.; Yang, J. Reversible Multi-Electron Redox Chemistry of π-Conjugated N-Containing Heteroaromatic Molecule-Based Organic Cathodes. *Nat. Energy* **2017**, *2*, 17074.
- 26. Hong, J.; Lee, M.; Lee, B.; Seo, D.-H.; Park, C. B.; Kang, K. Biologically Inspired Pteridine Redox Centres for Rechargeable Batteries. *Nat. Commun.* **2014**, *5*, 5335.
- 27. Lu, Y.; Hou, X.; Miao, L.; Li, L.; Shi, R.; Liu, L.; Chen, J. Cyclohexanehexone with Ultrahigh Capacity as Cathode Materials for Lithium-Ion Batteries. *Angew. Chem. Int. Eit.* **2019**, *58*, 7020-7024.
- 28. Luo, Z.; Liu, L.; Ning, J.; Lei, K.; Lu, Y.; Li, F.; Chen, J. A Microporous Covalent-Organic Framework with Abundant Accessible Carbonyl Groups for Lithium-Ion Batteries. *Angew. Chem. Int. Eit.* **2018**, *57*, 9443-9446.
- 29. Zhao, H.; Wang, J.; Zheng, Y.; Li, J.; Han, X.; He, G.; Du, Y. Organic Thiocarboxylate Electrodes for a Room Temperature Sodium-Ion Battery Delivering an Ultrahigh Capacity. *Angew. Chem. Int. Eit.* **2017**, *129*, 15536-15540.
- 30. Dou, C.; Ding, Z.; Zhang, Z.; Xie, Z.; Liu, J.; Wang, L. Developing Conjugated Polymers with High Electron Affinity by Replacing a C-C Unit with a B←N Unit. *Angew. Chem. Int. Eit.* **2015,** *54*, 3648-3652.
- 31. Ma, T.; Zhao, Q.; Wang, J.; Pan, Z.; Chen, J. A Sulfur Heterocyclic Quinone Cathode and a Multifunctional Binder for a High-Performance Rechargeable Lithium-Ion Battery. *Angew. Chem. Int. Eit.* **2016**, *55*, 6428-6432.
- 32. Van Wart, H. E.; Lewis, A.; Scheraga, H. A.; Saeva, F. D. Disulfide Bond Dihedral Angles from Raman Spectroscopy. *P. Natl. Acad. Sci. USA* **1973,** *70*, 2619-2623.
- 33. Chen, X.; Wang, H.; Yi, H.; Wang, X.; Yan, X.; Guo, Z. Anthraquinone on Porous Carbon Nanotubes with Improved Supercapacitor Performance. *J. Physic. Chem. C* **2014**, *118*, 8262-8270.
- 34. Coyle, C. M.; Chumanov, G.; Jagodzinski, P. W. Surface-Enhanced Raman Spectra of the Reduction Product of 4-Cyanopyridine on Copper Colloids. *J. Raman Spectrosc.* **1998**, *29*, 757-762.

- 35. Smith, A. M.; Schallmoser, G.; Thoma, A.; Bondybey, V. E. Infrared Spectral Evidence of N = C C = C N = C: Photoisomerization of N = C C = C C = N in an Argon Matrix. *J. Chem. Physic.* **1993**, *98*, 1776-1785.
- 36. Peralta, J.; Ogliaro, F.; Bearpark, M.; Heyd, J.; Brothers, E.; Kudin, K.; Staroverov, V.; Kobayashi, R.; Normand, J.; Raghavachari, K. Gaussian 09, Revision D. 01. Gaussian, Inc.: Wallingford, CT: **2013**.
- 37. Luo, C.; Wang, J.; Fan, X.; Zhu, Y.; Han, F.; Suo, L.; Wang, C. Roll-to-Roll Fabrication of Organic Nanorod Electrodes for Sodium Ion Batteries. *Nano Energy* **2015**, *13*, 537-545.
- 38. Brezesinski, T.; Wang, J.; Tolbert, S. H.; Dunn, B. Ordered Mesoporous α-MoO₃ With Iso-Oriented Nanocrystalline Walls for Thin-Film Pseudocapacitors. *Nat. Mater.* **2010,** *9*, 146.
- 39. Kim, H.-S.; Cook, J. B.; Lin, H.; Ko, J. S.; Tolbert, S. H.; Ozolins, V.; Dunn, B. Oxygen Vacancies Enhance Pseudocapacitive Charge Storage Properties of MoO_{3-x}. *Nat. Mater.* **2017**, *16*, 454.
- 40. Kostić, R.; Raković, D.; Stepanyan, S.; Davidova, I.; Gribov, L. Vibrational Spectroscopy of Polypyrrole, Theoretical Study. *J. Chem. Phys.* **1995**, *102*, 3104-3109.
- 41. Zarbin, A. J.; De Paoli, M.-A.; Alves, O. L. Nanocomposites Glass/Conductive Polymers. *Synthetic Met.* **1999**, *99*, 227-235.
- 42. Gao, X.-W.; Deng, Y.-F.; Wexler, D.; Chen, G.-H.; Chou, S.-L.; Liu, H.-K.; Shi, Z.-C.; Wang, J.-Z. Improving the Electrochemical Performance of the LiNi_{0.5}Mn_{1.5}O₄ Spinel by Polypyrrole Coating as a Cathode Material for the Lithium-Ion Battery. *J. Mater. Chem. A* **2015**, *3*, 404-411.